LETTER

Anomalous Hall effect of the quasi-two-dimensional weak itinerant ferromagnet $Cr_{4.14}Te_8$

A Letters Journal Exploring the Frontiers of Physics

December 2018

EPL, **124** (2018) 67005
doi: 10.1209/0295-5075/124/67005

www.epljournal.org

Anomalous Hall effect of the quasi-two-dimensional weak itinerant ferromagnet $Cr_{4.14}Te_8$

Jian Yan[1,2], Xuan Luo[1(a)], Gaoting Lin[1,2], Fangchu Chen[1,2], Jingjing Gao[1,2], Yan Sun[3], Ling Hu[1], Peng Tong[1], Wenhai Song[1], Zhigao Sheng[4,5], Wenjian Lu[1], Xuebin Zhu[1] and Yuping Sun[4,1,5(b)]

[1] *Key Laboratory of Materials Physics, Institute of Solid State Physics, Chinese Academy of Sciences Hefei, 230031, China*
[2] *University of Science and Technology of China - Hefei, 230026, China*
[3] *Institute of Physical Science and Information Technology, Anhui University - Hefei, 230601, China*
[4] *High Magnetic Field Laboratory, Chinese Academy of Sciences - Hefei, 230031, China*
[5] *Collaborative Innovation Center of Advanced Microstructures, Nanjing University - Nanjing, 210093, China*

received 24 August 2018; accepted in final form 11 December 2018
published online 15 January 2019

PACS 75.47.-m – Magnetotransport phenomena; materials for magnetotransport
PACS 75.50.Cc – Other ferromagnetic metals and alloys

Abstract – The anomalous Hall effect (AHE), a manifestation of the Hall effect driven by the Berry curvature, has numerous applications in spintronics and valleytronics. However, its realization in quasi-two-dimensional (quasi-2D) chromium tellurides remains puzzling. In this paper, we synthesize the $Cr_{4.14}Te_8$ single crystal and find that it shows weak itinerant ferromagnetic (FM) metallic behavior with a large magnetocrystalline anisotropy. At the same time, $Cr_{4.14}Te_8$ exhibits the AHE below the FM phase-transition temperature $T_C \sim 203$ K. By taking into account the scaling behavior between the anomalous Hall resistivity ρ_{xy}^A and the longitudinal resistivity ρ_{xx}, the origin of the AHE in this system is suggested to stem from the skew-scattering mechanism. Moreover, the possible magnetic ground state in $Cr_{4.14}Te_8$ has also been discussed to reveal the origin of AHE. Our results may be helpful for exploring the potential applications of these kinds of quasi-2D FM metals.

Introduction. – Since the monolayer graphene was successfully obtained by mechanical exfoliation, two-dimensional (2D) materials have attracted great interest due to the highly tunable physical properties and immense potential in scalable device applications [1–7]. However, the lack of band gap excludes its applications in spintronic devices, which requires other alternative 2D materials [8–12]. Recently, diverse alternatives with varying band gaps have been widely studied [9–12]. For example, in the family of transition metal dichalcogenides (TMDCs), the monolayer MoS_2 has been applied to spintronic devices due to its direct band gap and large spin-orbit coupling (SOC) [13–20]. In contrast, spintronic devices using 2D materials are still in their preliminary stage [21,22] because the long-range ferromagnetic (FM) order is strongly suppressed by thermal fluctuations in 2D materials systems according to the Mermin-Wagner theorem [23]. Thus, a lot of efforts have been devoted to finding magnetic materials for spintronics and attention is also extended to the study of magnetism of 2D materials [21,22,24–26].

Recently, the Cr-based 2D materials have received much attention for possible applications in spintronic devices due to the intrinsically long-range FM order [24–26]. Monolayer $CrGeTe_3$ exhibits FM ordering temperature (T_C) at $\sim$ 20 K, and it increases to $\sim$ 61 K in the bulk [24]. Moreover, another FM semiconductor, CrI_3, which exhibits the characteristic of the layer-dependent magnetic behavior may be a promising candidate for new magneto-optoelectronic devices [25]. However, the low T_C of the Cr-based 2D materials (below 70 K) restricts their possible applications. Actually, the binary chromium tellurides family $Cr_{1-x}Te$, *i.e.*, CrTe ($x = 0$), Cr_2Te_3 ($x = 0.33$), Cr_3Te_4 ($x = 0.25$), Cr_5Te_8 ($x = 0.375$), $Cr_{0.62}Te$ ($x = 0.38$) and $CrTe_2$ ($x = 0.5$), present FM metallic ground states [27–36]. According

(a)E-mail: xluo@issp.ac.cn
(b)E-mail: ypsun@issp.ac.cn

to the neutron diffraction measurements and photoemission spectroscopy, the concentration of metal vacancy (x) is important for the magnetic properties of these compounds [36]. More interestingly, the T_C of these compounds ranges from 170 K to 360 K, which is around the room temperature [27,35,36]. They present different crystalline structures. $CrTe_2$ ($x = 0.5$) exhibits a layered structure with T_C around 310 K [35], while $Cr_{1-x}Te$ crystals, for $x < 0.1$, crystallize as hexagonal NiAs type structures, and Cr_2Te_3 ($x = 0.33$) and Cr_3Te_4 ($x = 0.25$) form the monoclinic and trigonal structures with some Cr vacancies occupied randomly in alternate transition metal layers. When $0 < x < 0.25$, T_C is above the room temperature from 317 K to 360 K, while for $0.25 < x < 0.33$, their T_C is lower than 170 K. On the other hand, because of the itinerant nature of the Cr d electrons in these system, the observed saturation magnetization is much smaller than the calculated results using the ionic model by taking the spin canting into consideration for Cr_3Te_4 ($x = 0.25$), Cr_5Te_6 ($x = 0.166$) and Cr_7Te_8 ($x = 0.125$). And for Cr_2Te_3 ($x = 0.33$), the ordered magnetic moment via the neutron diffraction is 2.65–2.70 μ_B which is also smaller than the calculated 3 μ_B [29,37]. Furthermore, for $Cr_{0.62}Te$ ($x = 0.38$), it shows a crossover behavior in the magnetic interaction from short-range order to long-range order with an extension from two to three dimensions at $T_C \sim 230$ K based on critical behavior characterization. Thus, we can find non-negligible interlayer coupling and strong electron-electron correlation due to the hybridization between the Cr 3d and Te 5p bands [34], which has been confirmed by the angle-resolved photoemission spectroscopy (ARPES) measurement [31]. Generally, the system with strong electron correlation usually presents some emergent and remarkable phenomena, which leads us to refocus on the $Cr_{1-x}Te$ single crystals. Therefore, we grew the quasi-2D $Cr_{4.14}Te_8$ ($x = 0.48$) single crystals and did detailed research by magnetic, electronic and thermal transport measurements. Interestingly, the anomalous Hall effect (AHE) is observed below the T_C and the linear scaling behavior between ρ_{xy}^A and ρ_{xx} is obtained. Further analysis implies that the skew-scattering mechanism dominates the origin of the AHE in $Cr_{4.14}Te_8$. Our results may help to understand the origin of AHE in other quasi-2D FM metals.

Experimental details. – The single crystal $Cr_{4.14}Te_8$ was grown by the self-flux technique with Cr : Te = 5 : 95 molar ratio. Cr (purity 99.95%, Alfa Aesar) and Te (purity 99.99%, Alfa Aesar) grains were put into an alumina crucible and sealed in a quartz ampoule under partial argon atmosphere. The sealed quartz ampoule was heated and soaked at 1000 °C for 10 hours, then cooled down to 500 °C for 100 hours. At this temperature, the quartz ampoule was very quickly taken out from the furnace and decanted with a centrifuge to separate $Cr_{4.14}Te_8$ single crystals from the Te flux. As shown in fig. 1(b), the size of the studied crystal is about $2.5 \times 2.5 \times 0.1\,\mathrm{mm}^3$ with

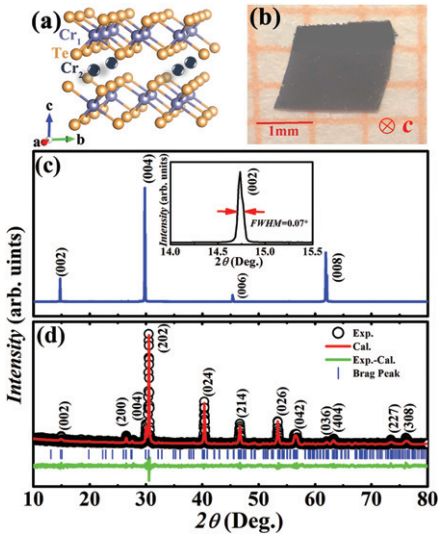

Fig. 1: (Color online) (a) The crystal structure of $Cr_{4.14}Te_8$. (b) The picture of the studied $Cr_{4.14}Te_8$ single crystal. The crystal size is approximately $2.5 \times 2.5 \times 0.1\,\mathrm{mm}^3$. (c) XRD patterns of the crystal measured on the (00l) surface. The inset presents a typical X-ray curve of the (002) Bragg peak. (d) Rietveld refined powder XRD patterns at room temperature for the crushed $Cr_{4.14}Te_8$ crystals. The vertical marks (blue bars) stand for the position of the Bragg peaks, and the solid line (green line) at the bottom corresponds to the difference between experimental and calculated intensities.

(00l) plane. Powder X-ray diffraction (XRD) experiments were performed by the PANalytical X'pert diffractometer using the Cu $K_{\alpha 1}$ radiation ($\lambda = 0.15406$ nm) at room temperature. Magnetization and electrical-transport measurements were carried out by using the Quantum Design magnetic property measurement system (MPMS-XL5) and the Physical Properties Measurement System for (PPMS-9 T) 1.8 K $< T <$ 400 K and the $H <$ 9 T. We performed the measurement of the specific heat by a heat-pulse relaxation method. A standard four-probe method and a five-probe method were used for both the longitudinal resistivity ρ_{xx} and transverse Hall resistivity ρ_{xy} measurements at different temperatures and magnetic fields, respectively. The applied magnetic field was perpendicular to the ab plane and the current was along the ab plane.

Results and analysis. – $Cr_{4.14}Te_8$ crystallizes as hexagonal structure with the space group $P\bar{3}m1$, which is isostructural with CrX_2 (X = Se, Te) [35,38,39]. As shown in fig. 1(a), Cr and Te atoms form the corner-sharing octahedral with few Cr ions intercalation between the $CrTe_2$ layers. Figure 1(b) presents the studied crystal with a flake-like shape and the largest natural surface is on ab plane. The quality of the $Cr_{4.14}Te_8$ single crystal is checked by the X-ray curve again and the full width at half-maximum (FWHM) of the (002) Bragg peak is 0.07°, as presented in the inset of fig. 1(c). The powder XRD data are collected on crushed $Cr_{4.14}Te_8$ single crystals at room temperature. Figure 1(d) presents the experimental

Table 1: Lattice parameters and two kinds of Cr atoms position in $Cr_{4.14}Te_8$ based on the Retiveld fitting.

Compound	a (Å)	b (Å)	c (Å)	c/a
$Cr_{4.14}Te_8$	7.7717	7.7717	11.9263	1.53
Atoms	x	y	z	Occu.
Cr in $CrTe_2$ layer	0	0	0.2461	1
Excess Cr	0	0	0.5032	0.072
Cr in $CrTe_2$ layer	0	0	0.7539	1

and the Rietveld refinement profiles of the XRD data using the FullProf software. It indicates that the powders are in single phase with hexagonal structure. And the lattice parameter is different from that in $CrTe_2$ [35]. On the other hand, the atoms position obtained by refinement shows that the excess Cr truly locates between the $CrTe_2$ layers, as shown in table 1.

The temperature-dependent longitudinal resistivity $\rho_{xx}(T)$ in the ab plane for $Cr_{4.14}Te_8$ is shown in fig. 2(a). The $\rho_{xx}(T)$ at zero field exhibits metallic behavior across the whole temperature range. Moreover, it shows a slope change at $T_C \sim 203\,\mathrm{K}$, which is determined from the $\mathrm{d}\rho_{xx}(T)/\mathrm{d}T$ curve, as shown in the left inset of fig. 2(a). As shown in the right inset of fig. 2(a), $\rho_{xx}(T)$ at low temperature can be well fitted by the Fermi liquid (F-L) formula ($\rho_{xx}(T) = AT^2 + \rho_0$ with $A = 0.01284\,\mu\Omega\,\mathrm{cm/K^2}$, $\rho_0 = 173.22\,\mu\Omega\,\mathrm{cm}$), which implies that the electron-electron scattering is dominant at low temperature. Figure 2(b) shows the variation of the zero-field specific heat ($C_P(T)$) with temperature. There is a broad peak around T_C, implying that the phase transition belongs to the second order in $Cr_{4.14}Te_8$ [40,41]. As shown in the inset of fig. 2(b), the plot of C_P/T *vs.* T^2 below 5 K can be well expressed by using following equation [42]:

$$C_P/T = \gamma_e + \beta T^2 + \delta T^4, \qquad (1)$$

where γ_e (Sommerfeld constant) is the electronic contribution, βT^2 is the phonon contribution, and δT^4 reflects the deviation term. As a result, the fitted values of the parameters γ_e, β, and δ are $49.6\,\mathrm{mJ/mol\,K^2}$, $3.54\,\mathrm{mJ/mol\,K^4}$, and $1.21\times10^{-4}\,\mathrm{mJ/mol\,K^6}$, respectively. The Debye temperature is determined by $\Theta_D = [(n \times 1.94\times10^6)/\beta]^{1/3} = 192\,\mathrm{K}$ (where n is the number of atoms in a unit cell). Generally, the value of the Kadowaki-Woods ratio (R_{KW}), defined as $R_{KW} = A/\gamma_e^2$ (where $A = 0.01284\,\mu\Omega\,\mathrm{cm/K^2}$ is the T^2-term coefficient of F-L fitting), is a well-known measurement of the electron correlation strength [43]. And the calculated R_{KW} of this system is $0.52\times10^{-5}\,\mu\Omega\,\mathrm{cm/(mJ/mol\,K)^2}$, which is 0.52 times the universal value of $a_0 = 1.0\times10^{-5}\,\mu\Omega\,\mathrm{cm/(mJ/mol\,K)^2}$, indicating $Cr_{4.14}Te_8$ is a weak correlated electron system [43]. Temperature-dependent magnetic susceptibility $\chi_c(T)$ and $\chi_{ab}(T)$ with zero-field-cooling (ZFC) and field-cooling (FC) modes at $\mu_0 H = 0.1\,\mathrm{T}$ for H // c and H // ab are shown in figs. 2(c) and (d), respectively. We

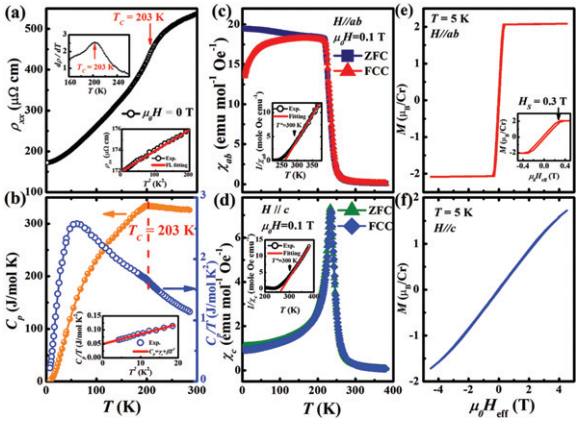

Fig. 2: (Color online) (a) Temperature-dependent longitudinal resistivity $\rho_{xx}(T)$ of a $Cr_{4.14}Te_8$ single crystal at zero field and $\mu_0 H = 8\,\mathrm{T}$ along the c-axis. Inset (i): left side: $\mathrm{d}\rho/\mathrm{d}T$ *vs.* T. Inset (ii): the F-L fitting of the $\rho_{xx}(T)$ at zero field. (b) The specific heat $C_P(T)$ and the C_P/T *vs.* T. Inset: C_P/T *vs.* T^2 at low temperature. The red solid line is the fitting result according to $C_P/T = \gamma_e + \beta T^2 + \delta T^4$. (c) and (d): temperature-dependent magnetization of the $Cr_{4.14}Te_8$ single crystal under ZFC and FC modes with the applied magnetic field $\mu_0 H = 0.1\,\mathrm{T}$. The inset shows the $\chi^{-1}(T)$ and the red solid lines are the fitting results according to the Curie-Weiss law. (e) and (f): the effective field dependence of magnetization $M(\mu_0 H)$ with $\mu_0 H//ab$ and $\mu_0 H//c$, respectively. The inset of panel (e) presents the H-dependent M at small scale, H_S corresponds to the saturation field.

observed a paramagnetic (PM)-FM transition that occurs around $T_C \sim 210\,\mathrm{K}$ by the deviation of the susceptibility, which is consistent with the result of the resistivity measurement. Usually, the susceptibility above T_C can be well described by the Curie-Weiss law. However, we find that the fitting curves deviate from the straight lines around $T^* \sim 300\,\mathrm{K}$ and are much higher than T_C, implying that there exists a possible magnetic correlation above T_C in this system. The parameters obtained from the fitting of the Curie-Weiss law are $C = 9.48$, $\theta_{CW} = 259.72\,\mathrm{K}$ and $C = 8.614$, $\theta_{CW} = 270\,\mathrm{K}$ for H // c and H // ab, respectively, indicating FM interactions in both directions. And the effective moments are determined to be $\mu_{eff} \sim 2.1\,\mu_B$ ($H//c$) and $\mu_{eff} \sim 2.0\,\mu_B$ ($H//ab$) per Cr ion. Moreover, the temperature dependence of magnetization $M(T)$ and isothermal magnetization $M(\mu_0 H)$ curves below T_C as shown in the main panel and the inset of figs. 2(c) and (d) show a strong magnetocrystalline anisotropy and the easy magnetization direction is the c-axis. Here, $\mu_0 H_{eff} = \mu_0(H - N_d M)$, where N_d is the demagnetization factor. A method devoted to calculating N_d in a rectangular FM prism was used, with detailed analysis given in ref. [43]. And we calculated that N_d is 0.21 in our system. For $H//c$, the saturation field H_S is around 0.3 T, however, for $H//ab$, M is not saturating up to 4.5 T, as shown in figs. 2(e) and (f). Higher $\mu_0 H$ measurements are desired to confirm the saturation behavior in the future. The strong magnetocrystalline anisotropy

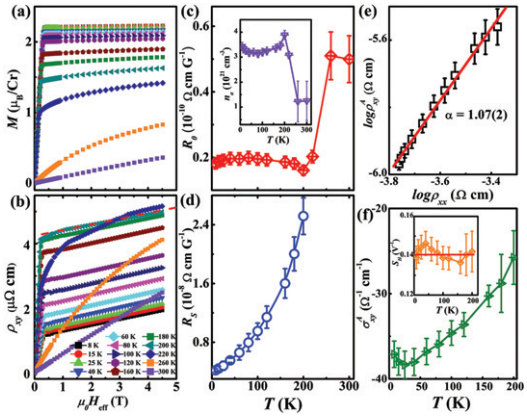

Fig. 3: (Color online) (a) and (b): magnetization and Hall resistivity $\rho_{xy}(\mu_0 H)$ as a function of magnetic induction $\mu_0 H$ for the $Cr_{4.14}Te_8$ single crystal at various temperatures with $H//c$, respectively. The red dashed line in (b) is the linear fit of $\rho_{xy}(\mu_0 H)$ in the high-$\mu_0 H$ region when $T \sim 200\,\mathrm{K}$. (c) and (d): temperature-dependent fitted $R_0(T)$ and $R_S(T)$ from $\rho_{xy}(\mu_0 H, T)$ curves using eq. (2). Inset of (c): derived $n_a(T)$ from R_0(T). (e) Plot of $\log\rho^A_{xy}(T)$ *vs.* $\log\rho_{xx}(T)$. The red solid line is the fit using $\rho^A_{xy} = \beta\rho^\alpha_{xy}$. (f) The anomalous Hall conductivity $\sigma^A_{xy}(T)$ as a function of temperature. Inset: temperature dependence of $S_H(T)$.

behavior has also been observed in other 2D FM materials, such as $CrXTe_3$ (X = Si, Ge) [44], and Fe_3GeTe_2 [45], and so on. Then, we calculate the Rhodes-Wohlfarth ratio (RWR) for $Cr_{4.14}Te_8$, which is defined as P_c/P_s with P_c obtained from the effective moments $P_c(P_c+2) = P^2_{eff}$ and P_s is the saturation moment obtained in the ordered state [46]. RWR is 1 for a localized system and is larger than 1 in an itinerant system. For $Cr_{4.14}Te_8$, the obtained RWR is about 2.56 for $H//c$, meaning a weak itinerant FM character of the studied system.

Figure 3(a) shows the effective field dependence of magnetization $M(\mu_0 H)$ at various temperatures between 8 and 300 K for $H//c$. For $T < T_C$, the $M(\mu_0 H)$ is a typical behavior for a ferromagnet with a rapid increase in low field regions and a saturation in higher fields. The saturation magnetization M_S decreases with increasing temperature. As for the Hall measurement, in order to eliminate the ρ_{xx} mixture, we measured the Hall resistivity both in positive field ($\rho_{xy}(+)$) and negative field ($\rho_{xy}(-)$). And then $\rho_{xy}(\mu_0 H) = (\rho_{xy}(+) - \rho_{xy}(-))/2$. The Hall resistivity $\rho_{xy}(\mu_0 H)$ data for the $Cr_{4.14}Te_8$ single crystal at various temperatures are shown in fig. 3(b). The $\rho_{xy}(\mu_0 H)$ increases quickly to certain saturated values at low $\mu_0 H$ regions below $T_C \sim 220\,\mathrm{K}$. By increasing $\mu_0 H$ forwardly, the $\rho_{xy}(\mu_0 H)$ increases slightly, while the $\mu_0 H$ dependence of $\rho_{xy}(\mu_0 H)$ is almost linear, *i.e.*, the $\rho_{xy}(\mu_0 H)/\mu_0 H$ is constant, which indicates that there is an AHE observed in $Cr_{4.14}Te_8$ [47,48].

Conventionally, the total Hall effect given by the Hall resistivity ρ_{xy}, is composed as

$$\rho_{xy} = \rho^O_{xy} + \rho^A_{xy} = R_0 B + R_S \mu_0 M, \qquad (2)$$

where ρ^O_{xy}, ρ^A_{xy}, R_0 and R_S are the ordinary Hall resistivity, the anomalous Hall resistivity, the ordinary Hall coefficient and the anomalous Hall coefficient, respectively. The values of R_0 and ρ^A_{xy} in principle can be determined from the linear fitting of the $\rho_{xy}(\mu_0 H)$ curves at saturation regions. The slope and y-axis intercept corresponds to the R_0 and ρ^A_{xy}, respectively. The R_S can be obtained by the second term of eq. (2), which is shown in figs. 3(c) and (d). Both the $R_0(T)$ and the $R_S(T)$ are positive. The former confirms that the hole-type carriers are dominated in this system, and the carriers concentration n_a ($R_0 \sim 1/n_a q$) is around $3 \times 10^{21}\,\mathrm{cm}^{-3}$, as presented in the inset of fig. 3(c). The $R_0(T)$ shows a mild temperature dependence below T_C, and when $T > T_C$, the value of R_0 becomes larger. Figure 3(e) presents the scaling behavior of ρ^A_{xy} *vs.* ρ_{xx}. By using the formula $\rho^A_{xy} = \beta\rho^\alpha_{xx}$, the fitting $\alpha = 1.07(2)$ across the whole temperature region is below that in T_C. The nearly linear relationship between ρ^A_{xy} and ρ_{xx} clearly indicates that the extrinsic skew-scattering mechanism dominates the AHE in $Cr_{4.14}Te_8$ rather than the intrinsic Karplus-Luttinger (KL) or extrinsic side-jump mechanism which give the quadratic relationship between ρ^A_{xy} and ρ_{xx} [47,48]. Furthermore, large anomalous Hall conductivity σ^A_{xy} ($\approx -\rho^A_{xy}/\rho^2_{xx} = R_S\mu_0 M/\rho^2_{xx}$) is observed in this system, which may be useful for various applications including in Hall devices in spintronics [21,22]. Temperature-dependent σ^A_{xy} is shown in fig. 3(f). The σ^A_{xy} is around $35\,\Omega^{-1}\,\mathrm{cm}^{-1}$, which shows a moderate temperature-dependent property. Several theoretical models and experiments have been done for unifying the origin of the large Hall conductivity in different systems [49,50]. For a metal with clean limit, the σ^A_{xy} is linearly dependent with σ_{xx}, and σ^A_{xy} is nearly a constant in some moderately dirty systems. Comparing the σ^A_{xy} and σ_{xx}, $Cr_{4.14}Te_8$ belongs to a moderately dirty system due to the intercalated Cr ions in disorder. In the inset of fig. 3(f), a scaling coefficient $S_H = \mu_0 R_S/\rho^2_{xx} = -\sigma^A_{xy}/M$, is nearly constant and independent of temperature. And the value of S_H is comparable with that in those traditional itinerant ferromagnets, such as *bcc* Fe and Ni [51,52]. Table 2 shows the comparison of some Hall effect parameters in some typical ferromagnets with different structures and ground states.

Let us try to understand the origin of AHE in $Cr_{4.14}Te_8$. Firstly, we briefly summarize the different mechanisms to understand the origin of AHE. Generally, the built-up electric field E_{Hall} compensates for the transverse flow of the carriers, which is deflected by the Lorentz force (see fig. 4(a)). This phenomenon, the so-called ordinary Hall effect, gives rise to the Hall voltage U_{Hall} being linearly proportional to the magnetic field B. However, in the systems with SOC or spontaneous FM polarization, the charge carriers gain an additional transverse momentum (fig. 4(c)). Consequently, the built-up Hall voltage attains a component U_{AHE}, the so-called anomalous

Table 2: Hall effect parameters in some ferromagnets. The ground states, the Hall effect temperature (T), the carrier concentration (n), hole (+) and electron (−), the anomalous Hall conductivity σ_{xy}^A and the coefficient $S_H = \mu_0 R_S/\rho^2$, indicating the relationship between σ_{xy}^A and M.

Materials	Ground states	T (K)	n (10^{21} cm^{-3})	σ_{xy}^A $(\Omega\text{cm})^{-1}$	S_H (V^{-1})	Ref.
$Cr_{4.14}Te_8$	FM	203	3	−35	0.14	this work
CrO_2	FM(skyrmion)	383		−40		[53]
Fe_3Sn_2	FM(kagome)	350	20	−400(< 100 K) −170(> 100 K)	0.04–0.09	[47]
Fe_xTaS_2	FM(hedgehog)	< 50	8–14			[54]
Fe(bcc)	FM	298	34	20.9	0.06	[51]
Ni	FM	293	−11	-6.6×10^3	−0.14	[52]
$CuCr_2Se_4$	FM	430	7.2	20		[55]
MnSi	FM(skyrmion)	< 29.5	5.9		−0.19	[56]
$La_{0.7}Sr_{0.3}CoO_3$	FM	2	6		0.06	[57]
$Nd_2Mo_2O_7$	FM(frustrated)	40		21(H//(100)) 8(H//(111))		[58]

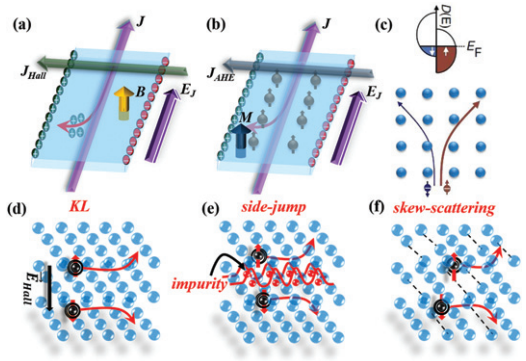

Fig. 4: (Color online) (a) and (b): the Hall voltage is built in applying the magnetic field B due to the Lorentz force and due to spin-orbit coupling (SOC) in ferromagnetic materials with a net magnetization M. (c) Appearance of the anomalous Hall effect because electrons deflected by the field of spontaneous magnetic moments in clean ferromagnetic metals. (d)–(f) The three schematic diagram dominated the Anomalous Hall effect, the intrinsic KL theory, the intrinsic side-jump mechanism and the extrinsic skew-scattering mechanism, respectively.

Hall component [59], originating from the SOC and being proportional to the magnetization M (fig. 4 (b)) [60,61]. So far, three mechanisms responsible for AHE have been widely accepted: the KL theory [62], the side-jump [63] and the skew-scattering mechanism [64]. The schematics are shown in figs. 4(d)–(f). Common to most of the materials class with AHE is the scaling behavior between the anomalous Hall resistivity ρ_{xy}^A and the longitudinal resistivity ρ_{xx}^α, where α is the scaling power factor. $\alpha = 2$ is for the intrinsic KL mechanism and the extrinsic side-jump mechanism and $\alpha = 1$ is for another extrinsic skew-scattering mechanism, respectively [62–64]. However, whether the AHE is originated purely from the extrinsic scattering or has an intrinsic contribution from the electronic band structure due to limited material systems and theoretical model so far has not been fully understood.

Secondly, for $Cr_{4.14}Te_8$, the electronic transport and magnetization analysis shows that it follows the skew-scattering mechanism. Figure 5(a) shows the diagram of the skew-scattering mechanism in the $Cr_{4.14}Te_8$ system. To understand the AHE of $Cr_{4.14}Te_8$, let us try to analyze the possible magnetic structure. Actually, $Cr_{4.14}Te_8$ can be considered to be intercalated $CrTe_2$, while some Cr ions intercalate into the van der Waals gap of $CrTe_2$ in disorder, which results in a more stable structure than that of metastable $CrTe_2$ [35]. Due to the disordered arrangement of intercalated Cr ions, the electrons are scattered asymmetrically contributing to the AHE in $Cr_{4.14}Te_8$. Figures 5(b) and (c) present the possible magnetic structure along ab plane and c-axis. Due to the unique crystal structure, there are two main magnetic exchange interactions (nearest-neighbor (NN) exchange interactions (J_1 and J_2)) existing in $Cr_{4.14}Te_8$. As shown in fig. 5(d), one is the direct exchange interaction originating from electron direct hopping between the NN Cr sites (upper panel in fig. 5(d)). Another one is the superexchange interaction, which is mediated through the Te ions, *i.e.*, two electrons excite from p orbits of Te ions to neighboring d ones of Cr ions (lower panel in fig. 5 (d), left side for intralayer, right side for interlayer). On the other hand, theoretical predictions show that the direct exchange interaction is AFM while the superexchange interaction is FM when the Cr-Te-Cr angle is close to 90° [65]. The similar competition of magnetic interactions is common in Cr-based materials, such as $CrSiTe_3$ and $CrGeTe_3$ and the superexchange interaction always play a dominant role in these Cr-based compounds [66]. As a result, the magnetic interaction of the ab plane in $Cr_{4.14}Te_8$ is determined by the competition between the direct exchange interaction and the superexchange interaction. Thus, it shows FM character along ab plane due to the domination of the superexchange

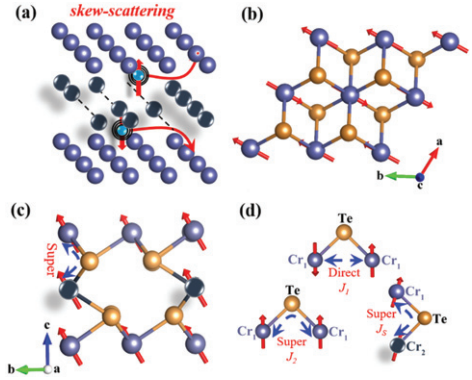

Fig. 5: (Color online) (a) The skew-scattering mechanism diagram in $Cr_{4.14}Te_8$. (b) and (c): the possible magnetic moments arrangement along the *ab* plane and the *c*-axis, respectively. (d) Illustrations of the Cr-Cr direct exchange (top panel), Cr-Te-Cr superexchange (left panel) and the Cr ($CrTe_2$ layers)-Te-Cr (intercalated) superexchange (right panel) interaction.

interaction in this system [39]. However, for the $Cr_{1-x}Te$ systems, there also exists strong hybridization between the Cr 3*d* band and the Te 5*p* band. The electron-correlation effect and the interlayer coupling plays an important role in the magnetic interactions [29,34,37]. Along the *c*-axis, because the intercalated Cr ions strengthen the magnetic and lattice coupling through Te ions, the angle of Cr-Te-Cr tends to be 90°. There also exists a superexchange interaction between the intercalated Cr ions and Cr ions in $CrTe_2$ layers (denoted by J_S) (the right side of fig. 5(d)) and the magnetic coupling is the FM coupling. Therefore, the origin of the AHE may result from the spontaneous FM polarization induced by the non-zero net magnetization due to the significant hybridization and electron correlation along the interlayer and intralayer in our system. Moreover, from the symmetry analysis, the net spontaneous magnetization breaks the time-reversal symmetry and also may induce the Berry curvature [48] and leads to the AHE which is from the FM interaction along the *c*-axis and the *ab* plane. However, the theoretical calculations and more experiments at low temperatures, such as the neutron scattering experiments on powders and single crystals of $Cr_{4.14}Te_8$, are needed to determine the magnetic ground state in the future.

Conclusion. – In summary, we systematically investigate the magnetic, electronic, and thermal properties of an itinerant FM metallic $Cr_{4.14}Te_8$ with a strong magnetocrystalline anisotropy. Then, we find that $Cr_{4.14}Te_8$ exhibits AHE below $T_C \sim 203\,\mathrm{K}$, and the scaling behavior $\rho_{xy}^A = \beta\rho_{xx}^\alpha$ reveals that it is the extrinsic skew-scattering mechanism rather than the intrinsic KL mechanism or the extrinsic side-jump mechanism that gives rise to the AHE. AHE maybe originates from the spontaneous FM polarization induced by the non-zero net magnetization, which is from the competition between the direct and superexchange Cr-Cr interaction due to the hybridization between the Cr 3*d* band and the Te 5*p* band and the strong electron correlation effect in $Cr_{4.14}Te_8$. Our observation is helpful to find out other quasi-2D FM metals with AHE character, which may be useful in spintronic devices applications.

* * *

The work was supported by the National Key Research and Development Program under contracts 2016YFA0300404, 2016YFA0401003 and 21017YFA0403600, the National Nature Science Foundation of China under contracts 11674326, 11874357, the Users with Excellence and Scientific Research Grant of Hefei Science Center of CAS (2018HSC-UE011), the Joint Funds of the National Natural Science Foundation of China and the Chinese Academy of Sciences' Large-Scale Scientific Facility under contract U1832141 and Key Research Program of Frontier Sciences, CAS (QYZDB-SSW-SLH015). The authors thank Dr Chen Sun for her assistance in editing the manuscript.

Additional remark: Recently, we became aware that Liu *et al.* [67] synthesized another Cr-Te compound Cr_5Te_8 ($T_C = 237\,\mathrm{K}$). Their conclusions regarding the extrinsic skew-scattering mechanism of AHE obtained by the linear scaling behavior $\rho_{xy}^A = \beta\rho_{xx}$ are consistent with our work.

REFERENCES

[1] Novoselov K. S., Geim A. K., Morozov S. V., Jiang D., Zhang Y., Dubonos S. V., Grigorieva I. V. and Firsov A. A., *Science*, **306** (2004) 666.
[2] Novoselov K. S., Geim A. K., Morozov S. V., Jiang D., Katsnelson M., Grigorieva I. V., Dubonos S. V. and Firsov A. A., *Nature (London)*, **438** (2005) 197.
[3] Zhang Y., Tan Y. W., Stormer H. L. and Kim P., *Nature (London)*, **438** (2005) 201.
[4] Geim A. K. and Novoselov K. S., *Nat. Mater.*, **6** (2007) 183.
[5] Castro Neto A. H., Guinea F., Peres N. M. R., Novoselov K. S. and Geim A. K., *Rev. Mod. Phys.*, **81** (2009) 109.
[6] Geim A. K. and Grigorieva I. V., *Nature (London)*, **499** (2013) 419.
[7] Chhowalla M., Shin H. S., Eda G., Li L. J., Loh K. P. and Zhang H., *Nat. Chem.*, **5** (2013) 263.
[8] Williams T. J., Aczel A. A., Lumsden M. D., Nagler S. E., Stone M. B., Yan J. Q. and Mandrus D., *Phys. Rev. B*, **92** (2015) 144404.
[9] Žutić I., Fabian J. and Das Sarma S., *Rev. Mod. Phys.*, **76** (2004) 323.
[10] MacDonald A., Schiffer P. and Samarth N., *Nat. Mater.*, **4** (2005) 195.
[11] Dietl T., *Nat. Mater.*, **9** (2010) 965.
[12] Deng Z., Jin C., Liu Q., Wang X., Zhu J., Feng S., Chen L., Yu R., Arguello C., Goko T. *et al.*, *Nat. Commun.*, **2** (2011) 422.
[13] Zhu Z. Y., Cheng Y. C. and Schwingenschlögl U., *Phys. Rev. B*, **84** (2011) 153402.
[14] Xiao D., Liu G.-B., Feng W., Xu X. and Yao W., *Phys. Rev. Lett.*, **108** (2012) 196802.

[15] Feng W., Yao Y., Zhu W., Zhou J., Yao W. and Xiao D., *Phys. Rev. B*, **86** (2012) 165108.
[16] Shan W. Y., Lu H. Z. and Xiao D., *Phys. Rev. B*, **88** (2013) 125301.
[17] Xu X., Yao W., Xiao D. and Heinz T. F., *Nat. Phys.*, **10** (2014) 343.
[18] Mak K. F., Lee C., Hone J., Shan J. and Heinz T. F., *Phys. Rev. Lett.*, **105** (2010) 136805.
[19] Sundaram R. S., Engel M., Lombardo A., Krupke R., Ferrari A. C., Avouris P. and Steiner M., *Nano Lett.*, **13** (2013) 1416.
[20] Splendiani A., Sun L., Zhang Y. B., Li T. S., Kim J., Chim C. Y., Galli G. and Wang F., *Nano Lett.*, **10** (2010) 1271.
[21] Han W., Kawakami R. K., Gmitra M. and Fabian J., *Nat. Nanotechnol.*, **9** (2014) 794.
[22] Chang C. Z., Zhang J., Feng X., Shen J., Zhang Z., Guo M., Li K., Ou Y., Wei P., Wang L. L. *et al.*, *Science*, **340** (2013) 167.
[23] Mermin N. D. and Wagner H., *Phys. Rev. Lett.*, **17** (1966) 1133.
[24] Gong C., Li L., Li Z. L., Ji H. W., Stern A., Xia Y., Cao T., Bao W., Wang C. Z., Wang Y. *et al.*, *Nature (London)*, **546** (2017) 265.
[25] Huang B., Clark G., Naavarro-Moratalla E., Klein D. R., Cheng R., Seyler K. L., Zhong D., Schmidgall E., McGuire M. A., Cobden D. H. *et al.*, *Nature (London)*, **546** (2017) 270.
[26] McGuire M. A., Clark G., KC S., Chance W. M., Jellison G. E., Cooper V. R., Xu X. D. and Sales B. C., *Phys. Rev. Mater.*, **1** (2017) 014001.
[27] Ipser H., Komarek K. L. and Klepp K. O., *J. Less-Common Met.*, **92** (1983) 265.
[28] Hessen B., Siegrist T., Palstra T., Tanzler S. M. and Steigerrwald M. L., *Inorg. Chem.*, **32** (1993) 5165.
[29] Hamasaki T. and Hashimoto T., *Solid State Commun.*, **16** (1975) 895.
[30] Akram M. and Nazar F. M., *J. Mater. Sci.*, **18** (1983) 423.
[31] Lukoschus K., Kraschinski S., Näther C., Bensch W. and Kremer R. K., *J. Solid State Chem.*, **177** (2004) 951.
[32] Huang Z. L., Bensch W., Mankovsky S., Polesya S., Ebert H. and Kremer R. K., *J. Solid State Chem.*, **179** (2006) 2067.
[33] Huang Z. L., Kockelmann W., Telling M. and Bensch W. A., *Solid State Sci.*, **10** (2008) 1099.
[34] Liu Y. and Petrovic C., *Phys. Rev. B*, **96** (2017) 134410.
[35] Freitas D. C., Weht R., Sulpice A., Remenyi G., Strobel P., Gay F., Marcus J. and Núñez-Reguerio M., *J. Phys.: Condens. Matter*, **27** (2015) 176002.
[36] Shimada K., Saitoh T., Namatame H., Fujimori A., Ishida S., Asano S., Matoba M. and Anzai S., *Phys. Rev. B*, **53** (1996) 7673.
[37] Andresen A. F., *Acta Chem. Scand.*, **24** (1970) 3495.
[38] Van Bruggen C. F., Haange R. J., Wiegers G. A. and De Boer D. K. G., *Physica B*, **99** (1980) 166.
[39] Lv H. Y., Lu W. J., Shao D. F., Liu Y. and Sun Y. P., *Phys. Rev. B*, **92** (2015) 214419.
[40] Wang A. F., Zaliznyak I., Ren W. J., Wu L. J., Graf D., Garlea V. O., Warren J. B., Bozin E., Zhu Y. M. and Petrovic C., *Phys. Rev. B*, **94** (2016) 165161.
[41] McGuire M. A., Garlea V. O., KC S., Cooper V. R., Yan J. Q., Cao H. B. and Sales B. C., *Phys. Rev. B*, **95** (2017) 144421.
[42] Kadowaki K. and Woods S. B., *Solid State Commun.*, **58** (1986) 507; Tong P., Sun Y. P., Zhu X. B. and Song W. H., *Phys. Rev. B*, **73** (2006) 245106.
[43] Aharoni A., *J. Appl. Phys.*, **83** (1998) 3432.
[44] Casto L. D., Clune A. J., Yokosuk M. O., Musfeldt J. L., Williams T. J., Zhuang H. L., Lin M. W., Xiao K., Hennig R. G., Sales B. C. *et al.*, *APL Mater.*, **3** (2015) 041515.
[45] Chen B., Yang J. H., Wang H. D., Imai M., Ohta H., Michioka C., Yoshimura K. and Fang M. H., *J. Phys. Soc. Jpn.*, **82** (2013) 124711.
[46] Wohlfarth E. P., *J. Magn. & Magn. Mater.*, **7** (1978) 113; Moriya T., *J. Magn. & Magn. Mater.*, **100** (1991) 261.
[47] Wang Q., Sun S. S., Zhang X., Pang F. and Lei H. C., *Phys. Rev. B*, **94** (2016) 075135.
[48] Nagaosa N., Sinova J., Onoda S., MacDonald A. H. and Ong N. P., *Rev. Mod. Phys.*, **82** (2010) 1539.
[49] Onoda S., Sugimoto N. and Nagaosa N., *Phys. Rev. B*, **77** (2008) 165103.
[50] Zhang S. F., *Phys. Rev. B*, **51** (1995) 3632.
[51] Dheer P. N., *Phys. Rev.*, **156** (1967) 637; Yao Y. G., Kleinman L., MacDonald A. H., Sinova J., Jungwirth T., Wang D. S., Wang E. and Niu Q., *Phys. Rev. Lett.*, **92** (2004) 037204.
[52] Jan J. P. and Gijsman H. M., *Physica*, **18** (1952) 339.
[53] Onada S., Sugimoto N. and Nagaosa N., *Phys. Rev. Lett.*, **97** (2006) 126602.
[54] Nozières P. and Lewiner C., *J. Phys. (Paris)*, **34** (1973) 901.
[55] Lee W. L., Watauchi S., Miller V. L., Cava R. J. and Ong N. P., *Science*, **303** (2004) 1647.
[56] Neubauer A., Pfleiderer C., Ritz R., Niklowitz P. G. and Böni P., *Physica B*, **404** (2009) 3163.
[57] Onose Y. and Tokura Y., *Phys. Rev. B*, **73** (2006) 174421.
[58] Taguchi Y., Oohara Y., Yoshizawa H., Nagaosa N. and Tokura Y., *Science*, **291** (2001) 2573.
[59] Hurd C. M., *The Hall Effect in Metals and Alloys* (Plenum, New York) 1972.
[60] Oveshnikov L. N., Kulbachinskii V. A., Davydov A. B., Aronzon B. A., Rozhansky I. V., Averkiev N. S., Kugel K. I. and Tripathi V., *Sci. Rep.*, **5** (2015) 17158.
[61] Liu X. J., Liu X. and Sinova J., *Phys. Rev. B*, **84** (2011) 165304.
[62] Karplus R. and Luttinger J., *Phys. Rev.*, **95** (1954) 1154.
[63] Berger L., *Phys. Rev. B*, **2** (1970) 4559.
[64] Smit J., *Physica*, **21** (1955) 877; **24** (1958) 39.
[65] Goodenough J. B., *Phys. Rev.*, **100** (1955) 564.
[66] Sivadas N., Daniels M. W., Swendsen R. H., Okamoto S. and Xiao D., *Phys. Rev. B*, **91** (2015) 235425.
[67] Yu L. and Petrovic C., *Phys. Rev. B*, **98** (2018) 195122.